Numerical Design of Double Quantum Coherence Filter for the Detection of *Myo*-Inositol *In vivo*

Yunjung Lee, Jinyoung Jung, Hyungjoon Noh, Ungsik Yu, Hyeonjin Kim

Purpose : A numerical method of designing a multiple quantum filter (MQF) is presented for the optimum detection of *myo*-inositol (mI), an important brain metabolite, by using *in vivo* proton nuclear magnetic resonance spectroscopy (^{1}H-MRS).

Materials and Methods : Starting from the characterization of the metabolite, the filter design includes the optimization of the sequence parameters such as the two echo times (TEs), the mixing time (TM), and the flip angle and offset frequency of the 3rd 90° pulse which converts multiple quantum coherences (MQCs) back into single quantum coherences (SQCs). The optimized filter was then tested both in phantom and in human brains.

Results : The results demonstrate that the proposed MQF can improve the signal-to-background ratio of the target metabolite by a factor of more than three by effectively suppressing the signal from the background metabolites.

Conclusion : By incorporating a numerical method into the design of MQFs in ^{1}H-MRS the spectral integrity of a target metabolite, in particular, with a complicated spin system can be substantially enhanced.

Index words : Magnetic resonance spectroscopy (MRS)
Multiple quantum filter (MQF)
Myo-inositol

Introduction

The cerebral level of *myo*-Inositol (mI) is known to vary with the progression of various diseases and disorders such as Alzheimer's disease (1-4), diabetes mellitus (5), Hepatic encephalophacy (6-9), depression (10) and bipolar (manic-depressive) disorder (11-14). Therefore, the precise quantification of the metabolite using *in vivo* nuclear magnetic resonance (NMR) technique may help diagnose and monitor patients with such diseases and disorders.

Point resolved spectroscopy (PRESS) and stimulated echo acquisition mode (STEAM) are the two most commonly used single voxel localization pulse sequences in *in vivo* proton magnetic resonance

JKSMRM 13:117-126(2009)
[1]Lee Gil Ya Cancer and Diabetes Institute, Gachon University of Medicine and Science,
Received; October 19, 2009, revised; November 26, 2009, accepted; December 5, 2009
Corresponding author : Hyeonjin Kim, Ph.D., Ungsik Yu, Ph.D., Lee Gil Ya Cancer and Diabetes Institute, Gachon University of Medicine and Science, 7-45, Songdo-dong, Yeonsu-gu, Incheon 406-840, Korea.
Tel. 82-32-899-6060, 6058 Fax. 82-32-899-6058 E-mail: hkim@gachon.ac.kr, ungsik@gachon.ac.kr

spectroscopy (^{1}H-MRS). STEAM has been more popular for the measurement of the metabolite as a result of the shorter echo times (TEs) attainable (2, 4, 5-8, 15-17). The use of short TEs, however, enhances not only the mI resonance at ~ 3.6 ppm, which is most widely used as a target peak of the metabolite for its dominant signal intensity over the other satellite peaks belonging to the molecule, but it also enhances those of background resonances such as the A multiplet of AMNPQ spin system of glutamate (Glu) and glutamine (Gln) (collectively referred to as Glx) at ~ 3.78 ppm, and taurine (Tau) at ~ 3.45 ppm. An enhancement of other source of unwanted background signal such as macromolecules (18-20) is an additional disadvantage of using short sequence timings. Therefore, a better signal yield of the target peak by shortening the sequences tends to be compensated with less precise outcome.

It is possible to establish optimum *long* sequence timings for both PRESS and STEAM for the effective suppression of those background resonances, while retaining an observable amount signal of mI (21). The suppression of macromolecule resonances is an additional benefit of using such long TEs as their T_2 values are known to be significantly shorter (18, 20). In the case of weakly-coupled spin systems or strongly-coupled ones with a restricted number of spins, the prediction of such optimum long pulse sequence timings can be achieved by referring to the product operator formalism (22) with an acceptable precision, but as mI consists of strongly-coupled 6-spins, an analytical method is impractical. By numerical solution of the density matrix (23), the establishment of such optimum long sequence timings can be achieved. Nonetheless, the problem of uncoupled glycine (Gly) overlapping with the target peak of mI cannot be resolved upon the use of these conventional pulse sequences. Although found in brain at a very low concentration with respect to that of mI (mI : Gly ~ 5 : 1 (24)), the presence of the Gly singlet exacerbates the precise quantification of the metabolite *in vivo*.

A difference spectra method (25, 26) might be an alternative for the removal of uncoupled spin resonances such as Gly. Although difference spectra methods can potentially retrieve a greater signal yield in the target peak, they have an intrinsic problem of sensitivity to the subject motion during acquisitions, which causes cancellation errors (27, 28). Furthermore, in the case of mI, the complicated evolution of the spin system facilitated by strong coupling Hamiltonian results in a rapid change in the lineshape and signal amplitude as a function of sequence timings. As a result, the use of difference spectra methods appears to be impractical in this case.

A double quantum filter (DQF) (23, 27, 28, 30-37) has been more useful than the difference spectra methods for the purpose of background suppression for the following reasons. First, combined (most commonly) with the PRESS sequence for the purpose of spatial localization, DQF becomes a single-shot method for data acquisition with less susceptibility to subject motion. Secondly, it provides a unique way of suppressing uncoupled metabolites by taking advantage of the fact that uncoupled spin systems cannot evolve into multiple quantum states. However, due to the inherent problem of poor signal yield with the sequence, the design of DQF requires more sophistication in the optimization procedure for a variety of sequence parameters (23) such as TEs, mixing time (TM), and the tip angle, the frequency offset and the duration of the third 90° pulse, which converts multiple quantum coherences (MQCs) during the TM period back into anti-phase coherences (APCs). Combined with the complexity of the mI spin system, the optimal design of DQF for mI is not a trivial task. Lei et al. (29) achieved the optimization of DQF for Tau, which is strongly-coupled A_2B_2 spin system, by extrapolating equations of spin evolution based on the previously published analytic solutions for the AB system of citrate in terms of product operators (38). However, to the best of our knowledge, such an analytic basis for the prediction of the response of mI to DQF is not available to date.

In this report, we tackle the problem of optimizing DQF for the complicated spin system of mI by using the numerical method (23). Of special importance in the optimization procedure are the effective removal of uncoupled Gly and neighboring metabolites with coupled spins such as Glx and Tau, while still retaining an observable amount of filtered mI signal.

Materials and Methods

Spectral Characteristics of mI and Its Background Metabolites

The mI molecule has a chair conformation with a symmetry about the axis that connects A spin (H(2)) and P spin (H(5)) (11, 39). The mI spin system can be termed as AM_2N_2P at 3T, based on the ratio of the coupling constant to the difference in chemical shift in Hz (J/δ) between coupled spins, e.g., $[J/\delta]_{AM} \sim 0.04$ (weak-coupling), $[J/\delta]_{MN} \sim 0.97$ (strong-coupling) and $[J/\delta]_{NP} \sim 0.21$ (strong-coupling). The chemical shifts and the coupling constants of the mI spin system (40) were summarized in Table 1.

The resonances of mI are grouped into three multiplets. Among them, the mI triplet at ~ 3.3 ppm, which is contributed by P spin, is almost completely overlapped with resonances from Tau and choline (Cho). Therefore, the possibility of using it as a target peak is excluded in conjunction with its low signal amplitude with respect to the central multiplet at ~ 3.6 ppm. Similarly, the A spin resonance at ~ 4.1 ppm overlaps with Cr and a small amount of lactate (Lac).

Table 1. Spectral Characteristics of *Myo*-Inositol Spin System

Proton No.	H(2)	H(1),H(3)	H(4),H(6)	H(5)
Spin Species	A	M_1,M_2	N_1,N_2	P
Chemical Shift (ppm)	4.06	3.54	3.62	3.28
J-Coupling Constant		$J_{M1A} = J_{AM2} = 2.7$ $J_{M2N1} = 9.9$ $J_{M1N2} = 9.8$ $J_{N1P} = J_{PN2} = 9.2$		

Table 2. Number of Single Quantum Anti-phase Coherences (APCs) Converted by the Third 90° Pulse. Three different excitation schemes are shown. Only those APC terms with transverse M or N magnetization were counted, which ultimately contribute to the target peak of mI at ~ 3.6 ppm (DQC_{real}: real term of double quantum coherence, DQC_{imag}: imaginary term of double quantum coherence)

Spin species excited by 3rd 90° pulse	DQC (imag.) ⇓ APC	DQC (real) ⇓ APC	Total APCs
P	4	4	8
M, N, P	16	0	16
A, M, N, P	20	0	20

This peak is usually unobservable *in vivo* with unedited pulse sequences such as PRESS and STEAM due to its spectral proximity to the strong water signal. The quartet-like, central multiplet at ~ 3.6 ppm (M_2N_2 spin resonances) is assigned to be the target peak for its dominance in amplitude over the two other multiplets, although it does have overlaps with Glx and Tau as well as with Gly. Due to low concentrations relative to mI in normal human brain, some of the background metabolites whose resonances lie between the A and the P multiplets are not considered in this study. They are alanine (~ 3.78 ppm), glucose (~ 3.75 ppm and 3.4 ppm) and syllo-Inositol (~ 3.35 ppm).

Sequence Optimization

A generic DQF sequence is shown in Fig. 1, in which PRESS was incorporated into the sequence for the purpose of spatial localization. It is comprised of three 90° r.f pulses and two 180° pulses. The optimization of each radio-frequency (r.f.) pulse in the sequence was achieved by using MATPULSE software (41) written in MATLAB™ (Mathworks Inc., Nadick, USA). The first 90° pulse is an optimized sinc pulse which is ~ 3 ms in duration and ~ 4000 Hz in bandwidth. For the second 90° pulse that generates MQCs, a rectangular hard pulse was chosen with its duration as short as 250 μs to minimize additional intra-pulse evolution of coherences, namely, the mixing of coherences (23, 42,

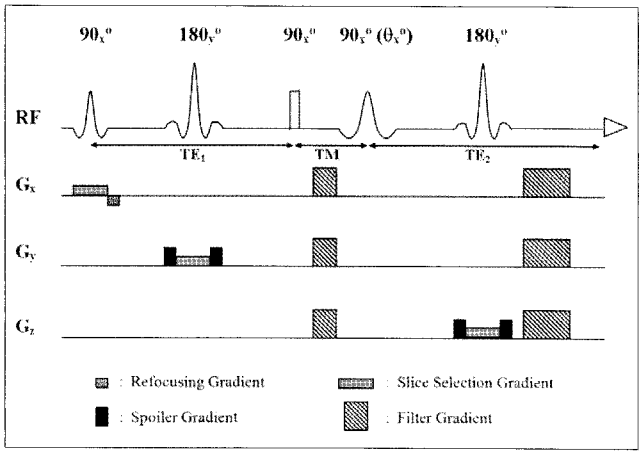

Fig. 1. A generic DQF sequence. It consists of three 90° and two 180° r. f. pulses. The filtering of a specific order of coherence is achieved by the second and the third 90° pulse in conjunction with a pair of filter gradients. The area of the second filter gradient is adjusted with respect to the first one, according to the level of coherence to be filtered out.

43). The optimization of the third 90° read pulse, a numerically optimized sinc-Gaussian pulse, includes consideration of the frequency offset, duration and tip-angle, which will be discussed below in detail. As for the two 180° pulses, an optimized sinc pulse was used for both slice selection and chemical shift refocusing with a duration of 3.5 ms and a bandwidth of ~ 1200 Hz. The length and amplitude of each slice selection gradient was calculated according to the size of a voxel. The duration of spoiler gradients for each 180° refocusing pulses was 2 ms with the maximal amplitude of 20 mTm^{-1}. The filter gradients were applied in all three directions with the length of G_1 = 3 ms and $G_2 = 2 \times G_1$ for double quantum selection, and the maximal amplitude of 20 mTm^{-1} for both G_1 and G_2. The net gradient vector, therefore, was oriented at the magic angle to facilitate the suppression of residual water signal resulting from the demagnetizing dipole-dipole interaction between water molecules in conjunction with a 16 step phase-cycling (23).

The determination of the optimum values for the offset frequency and bandwidth (or duration) of the third 90° read pulse preceded the optimization of TEs and TM. To determine the most appropriate excitation scheme by the read pulse an analysis was made by using the product operator formalism (22) where the optimization criterion was to produce the largest number of single quantum APCs (SQ-APCs) with at least one transverse M or N term that ultimately contributes to the target peak. The result is summarized in Table 2. The additional double-order terms that are produced during the TM period by involving more than one passive spin with the level of coherence unchanged e.g., $A_xM_{1x}N_{2z}$, were not included in the analysis for their negligible contribution to the final signal yield (see the source of variability section for detailed discussion). Since each DQC has two terms, namely a real and an imaginary term, the notation such as $DQC\{AM_1\}_{real}$ and $DQC\{AM_1\}_{imag}$ was used in the analysis to distinguish one from the other. Since the creation of the DQCs that involve two spins with no direct J-coupling between them but have a common coupling partner (e.g., DQC{AN}) is also possible in the case of strongly-coupled spin systems (42–44), such terms were also considered in the analysis. According to Table 2, exciting all spin species yields the largest number of SQ-APCs with at least one transverse M or N term. Therefore, the third 90° frequency selective pulse was tuned to excite all spin species of mI, while

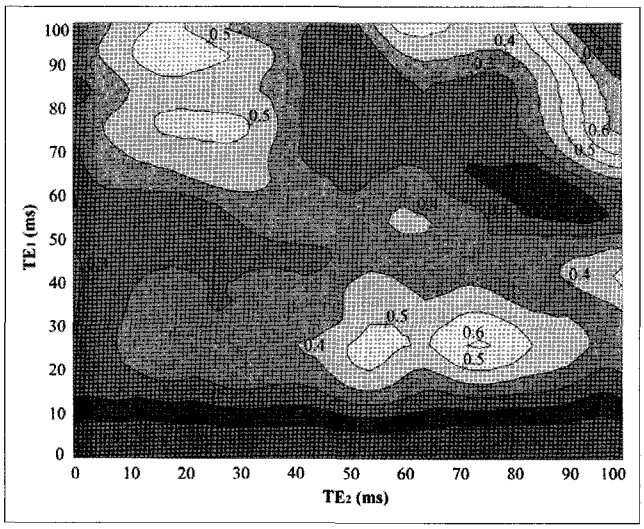

Fig. 2. The contour plot of the calculated signal intensity of the target peak of *myo*-Inositol in response to a DQF sequence for the determination of semi-optimum TE_1 and TE_2. Initially, TM was set to 5 ms. Also, the flip angle and the duration of the frequency selective r.f. pulse was set to 90° and 5 ms, respectively. No relaxation loss was assumed in the calculation. All indices were normalized to the maximum signal found at both TE_1 and TE_2 ~ 100 ms. A step size of 2 ms was used in the calculation for both TE_1 and TE_2.

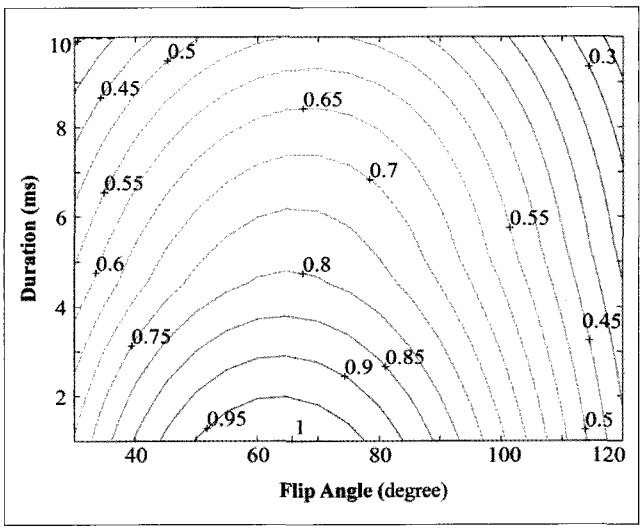

Fig. 3. The variation of the calculated signal intensity of the target peak of *myo*-Inositol as a function of the duration and the flip angle of the third 90° frequency selective pulse. No relaxation loss was assumed in the calculation. Also, the indices were normalized to the maximum signal found at the duration of 1 ms and the flip angle of ~ 65°.

leaving water resonance intact.

As the next step in the design of a DQF for mI editing, the optimization of TE_1 and TE_2 followed. With an initial value of 5 ms for TM, and 90° and 5 ms for the flip angle and duration of the read pulse, respectively, a contour plot of the signal intensity of the target peak of mI was produced (23) as shown in Fig. 2. It visualizes the variation in the signal intensity of the targeted peak as a function of TE_1 (vertical axis) and TE_2 (horizontal axis) in ms ({TE_1, TE_2}). No transverse relaxation was assumed in the calculation and all indices were normalized to the maximum appearing ~ {100,100} region in the Figure. Based on this preliminary contour plot and initial TM of 5 ms, the optimization of the tip angle and the duration of the third 90° read pulse was achieved by producing another contour plot as a function of those two sequence parameters as illustrated in Fig. 3. According to Fig. 3, the optimal flip angle is found to be ~ 65°, and the shorter the duration of the pulse is, the better the signal yield is. However, in consideration of the bandwidth issue of the pulse as described above, the initial duration of 5 ms was retained. Figure 4 was also used for the optimization of TM, which illustrates the dependence of the signal yield of the filter on the choice of TM. In practice, TM of 7 ms was used to accommodate the filter gradient during the mixing period.

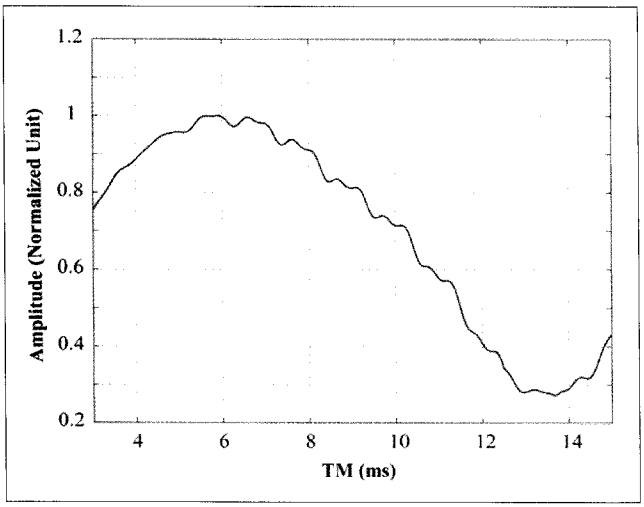

Fig. 4. The variation of the calculated signal intensity of the target peak of *myo*-Inositol as a function of TM. The amplitude was normalized to the maximum value that occurs at ~5.5 ms of TM. No relaxation loss was assumed in the calculation.

As the final step, all the parameters thus obtained were combined to produce another contour plot for the reoptimization of TE_1 and TE_2 (23). The contour plots for the A multiplets of Glx and for Tau were also produced for effective suppression of those neighboring metabolites.

Phantom and In Vivo Experiments

Two spherical phantoms (~ 5 cm in diameter ; pH = ~ 7) of aqueous solutions were made. One (phantom #1) contains mI + Cr and the other (phantom #2) mI + Glu + Gln + Tau + Cr + Gly at their relative physiological concentration ratio of normal human brain (1 : 1.3 : 0.6 : 0.5 : 1.1 : 0.2) (24, 45, 46). For both phantoms the concentration of mI was maintained at 50 mM. The Phantom #1 also contains 10 mM Cr to be used as a reference peak.

An 80-cm bore 3T magnet (Magnex Scientific PLC, Abingdon, UK) was used for all tests with a home-built 28-cm diameter quadrature birdcage coil for both transmission and reception. The spectrometer control was provided by a SMIS console (Surrey Medical Imaging Systems PCL, Guilford, UK). A total of 2048 data points were used for data acquisition. For phantom experiments, a voxel of 2.5 × 2.5 × 2.5 cm^3 was located at the isocenter of the phantom. For in vivo experiments, a voxel of 3.5 × 3.5 × 3.5 cm^3 was defined in the occipital region of the brain.

All post-data processing was conducted by using the spectrum analysis software (Specana) provided by SMIS. A linewidth broadening of ~ 7 Hz was applied for all spectra and signal intensity was measured thereafter. For the estimation of signal-to-background ratios (S/B), the target spectral region was chosen between 3.4 ppm and 3.75 ppm.

Results

Based on the contour plots obtained for M_2N_2 multiplet of mI, A multiplets of Glx and for Tau, the optimized sequence parameters for the DQF were determined to be ; TE_1 = 32 ms, TE_2 = 58 ms, TM = 7 ms, and the duration and the flip angle of the third 90° being 5 ms and ~ 65°, respectively, with the frequency offset of the pulse tuned to excites all spin species of mI.

The optimized filter for mI detection was tested first

in phantom experiments. Fig. 5 shows the response of the metabolites in (a) phantom #1 and in (b) phantom #2 to PRESS. The filtered spectra of mI are also shown (Fig. 5(d)) without, and (Fig. 5(e)) with, its background metabolites along with the calculated response (Fig. 5(c)). In comparison of Figs. 5(d) and (e), the A multiplet of Glx and Tau are observed to be effectively suppressed, while the MNPQ multiplets of Glx still persist over the range of the spectrum from 2.0 through 2.5 ppm. The lineshape and the signal amplitude of the mI target peak are all in accordance with one another, demonstrating complete removal of the uncoupled Gly from the target region. This is further supported by the observation that the Cr resonances at ~ 3.0 and ~ 3.9 in PRESS experiment (Fig. 5(b)) were completely eliminated in the filtered spectrum (Fig. 5(e)). The signal yield of mI in response to the optimized filter is estimated to be ~ 15% of that obtainable in PRESS experiment with the shortest timings of TE_1 = 18 and TE_2 = 16 ms. The S/B between 3.4 ppm and 3.75 ppm were ~ 4.8 for the optimized filter and ~ 1.5 for PRESS, an improvement by a factor of more than three in favor of the filter.

The performance of the optimized DQF was further tested in vivo and the result is shown in Fig. 6(b), which was taken from the occipital region of the human brain (a healthy 30 year-old male volunteer ; 3.5 × 3.5 × 3.5 cm^3; 512 averages). The lineshape of mI at ~ 3.6 ppm well matches that in phantom spectrum in Fig. 6 (a). In Fig. 6(b), the MNPQ multiplet of Glx at ~ 2.3 ppm (negative peak) is also well identified as in the phantom spectrum in (a). As well, no uncoupled peaks are observed such as water, Cr and N-acetylaspartate (NAA; ~ 2.0 ppm). Therefore, taking account of the relative abundance of those singlet resonaces, no leakage from Gly can be assured in the target region. Finally, since a total TE of 90 ms was used, the contamination of the target region by macromolecule resonances can be neglected (18, 20).

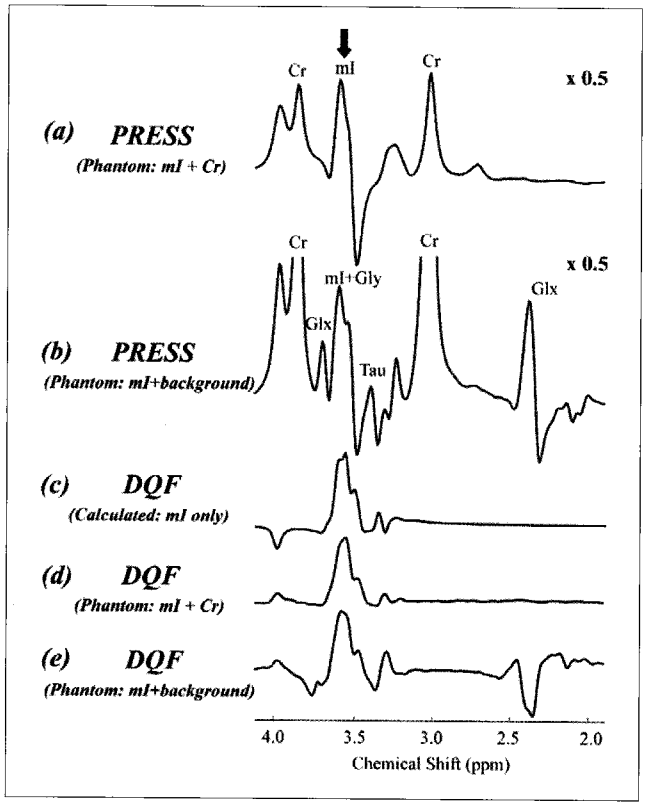

Fig. 5. The phantom response of *myo*-Inositol and its background metabolites to a PRESS and the optimized DQF. The response of mI to a PRESS at {TE_1 = 32 ms, TE_2 = 58 ms} is shown (**a**) without, and (**b**) with, background metabolites. The filtered mI signal is also shown (**d**) without, and (**e**) with, its background metabolites. The calculated spectrum is also shown in (**c**). The lineshape of the mI target multiplet matches close to one another in all filtered spectra. For all spectra, the linewidth was artificially broadened to ~7 Hz.

Discussion

The purpose of this study was to establish an optimal

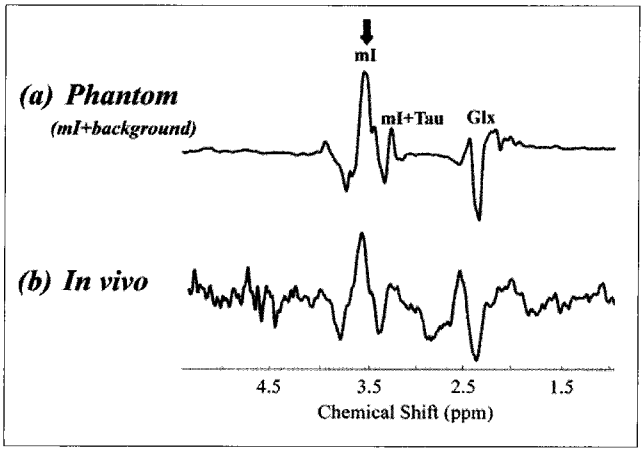

Fig. 6. The DQ-filtered spectra of the human brain. Shown in (**a**) is the phantom response of mI and its background metabolites to the optimized filter. The spectrum in (**b**) was taken from the occipital region of the brain of a 30 years old healthy male subject with a voxel size of 3.5 × 3.5 × 3.5 cm^3 and 512 averages (scan time ~ 27 min). In (b), the MNPQ multiplets of Glx at ~ 2.3 ppm is also identified.

condition in the design of DQF sequence for the detection of mI *in vivo*. The advantage of the filter sequence lies in its capability to suppress any uncoupled spin resonance, which is an important aspect in that the contamination of the target peak by uncoupled Gly was unavoidable in PRESS and STEAM even after the optimization of these conventional sequences. However, in addition to the intrinsic poor signal yield of a DQF and a variety of sequence parameters to be optimized, the difficulty in designing the filter for mI detection is exacerbated by the complexity of the mI spin system and its evolution. It was emphasized that the difference spectra method is not a practical alternative to DQF for the same reason, i.e., the rapid change in the line shape of mI as a function of sequence timings, which results from the strongly-coupled nature of the metabolite. As such, the prediction of the evolution of mI in response to a DQF sequence cannot be achieved in the conventional way, namely, the product-operator formalism. By using numerical solution of the density matrix, a methodical procedure for the design of a DQF sequence (23) was adopted in this study.

Among the sequence parameters to be optimized, the frequency offset of the third 90° read pulse was considered first in the optimization procedure, from which it was determined that all of the spin species of mI were to be excited by that pulse. However, it should be noted that for strongly-coupled spin systems the optimal spectral region to be excited by the third 90° pulse is also TE_2-dependent due to the active coherence transfer even during the inter-pulse delays (21, 23). Therefore, the analysis given herein should be used only as a guideline. Another excitation scheme may be possible such as the excitation of A and P spins by using a composite pulse (47, 48). But for the same reason, it does not necessarily enhance signal yield. Moreover, it may result in unwanted perturbation of other spectral region such as the excitation of water resonance. Therefore, the use of a composite pulse as the third 90° read pulse was not considered in this study.

The performance of the optimized filter was tested both in phantom and *in vivo*. The filter yield of mI target peak was estimated to be ~ 15 % with respect to that obtainable with PRESS at the shortest sequence timings. To overcome this relatively low signal yield of the filter, a rather large voxel size of 3.5 × 3.5 × 3.5 cm^3 was used in the human study. According to the product operator analysis with rectangular hard pulse approximation (22) a theoretical DQF signal yield is ~ 25% for weakly-coupled spin systems. However, there are a variety of signal loss mechanisms in practical MRS experiments. For instance, the use of shaped soft pulses alone can give rise to a substantial amount of signal loss and this signal reduction can be even worse for strongly-coupled spin systems (21, 23). In addition, the active coherence transfer throughout the filter sequence should be one of the mechanisms responsible for the lower filter yield of mI, e.g., the coherence transfer from the signal-contributing M or N spin species to A and P spins under the strong coupling Hamiltonian followed by unwanted proliferation of coherences into non-observable terms such as additional double order terms (21, 42, 43). As well, it should also be noted that although those DQ-filtered output reported in the literature range from ~ 25 to ~ 45 % (23, 27, 28, 30–32, 34, 35), some of these values (27, 28, 30, 35) were estimated with respect to that obtained with PRESS or STEAM at the same sequence timings used for DQF experiments instead of at the shortest sequence timing as in this study. Therefore, given that the J-modulation of coupled spin systems over TEs can lead to a substantial loss of signal, those relatively high filter yield in the previous studies should be carefully interpreted.

The suppression efficiency of the filter for other uncoupled resonances with relatively large signal intensity such as water, Cr and NAA, guaranteed the complete removal of the uncoupled Gly resonance from the target spectral region. It was also shown both in phantom and *in vivo* that the background metabolites with coupled spins were effectively suppressed. Therefore, despite the low signal yield, the numerically optimized filter in this study can find important applications in quantitative ^{1}H-MRS studies.

A new editing method was reported by Trabesinger et al. (49), namely, the single quantum coherence filtering. The sequence can simply be implemented by one additional 90° pulse at the first echo location in the conventional PRESS sequence. It filters out SQCs of strongly-coupled spin systems only, while suppressing those from weakly-coupled and the uncoupled spins. Intuitively, the application of the single quantum filter

(SQF) may be very suitable for the mI editing, since the weakly-coupled A spin multiplets of Glx and the uncoupled Gly singlet can effectively be removed by the nature of the sequence. This additional degree of freedom in the sequence optimization procedure may potentially be valuable in the mI editing.

Finally, the results shown here are specific to a magnetic field strength of 3T. Due to the changes in chemical shift difference (in Hz), the evolutionary picture of the mI spin system in response to the DQF will need to be redefined in a different magnetic field strength.

Conclusion

By incorporating a numerical method into the design of MQFs in 1H-MRS the spectral integrity of a target metabolite, in particular, with a complicated spin system can be substantially enhanced.

References

1. Moats RA, Ernst T, Shonk TK, Ross BD. Abnormal celebral metabolite concentrations in patients with probable Alzheimer disease. Magn Reson Med 1994;32:110-115
2. Miller BL, Moats RA, Shonk TK, Ernst T, Woolley S, Ross BD. Alzheimer disease: depection of increased cerebral myo-inositol with proton MR spectroscopy. Radiology 1993;187:433-437
3. Ross BD, Bluml S, Cowan R, Danielsen E, Farrow N, Gruetter R. In vivo magnetic spectroscopy of human brain: the biophysical basis of dementia. Biophys Chem 1997;68:161-172
4. Shonk T, Ross BD. Role of increased cerebral myo-inositol in the dementia of Down Syndrome. Magn Reson Med 1995;33:858-861
5. Kreis R, Ross BD. Cerebral metabolic disturbances in patients with subcute and chronic Diabetes Mellitus: detection with proton MR spectroscopy. Radiology 1992;184:123-130
6. Kreis R, Ross BD, Farrow NA, Ackerman Z. Metabolic disorders of the brain in chronic Hepatic Encephalopathy detected with H-1 MR spectroscopy. Radiology 1992;182:19-27
7. Naegele T, Grodd W, Viebahn R, Seeger U, Klose U, Seitz D, Kaiser S, Mader I, Mayer J, Lauchart W, Gregor M., Voigt K. MR imaging and ^{1}H spectroscopy of brain metabolites in Hepatic Encephalopathy: Time-course of renormalization after liver transplantation. Radiology 2000;216:683-691
8. Ross BD, Jacobson S, Villamil F, Korula J, Kreis R, Ernst T, Shonk T, Moats RA. Subclinical Hepatic Encephalopathy: proton MR spectroscopic abnormalities. Radiology 1994;193: 457-146
9. Moat RA, Lien YH, Filippi D, Ross BD. Decrease in cerebral inositols in rats and humans. Biochem J 1993; 295:15-18
10. Frey R, Metzler D, Fisher P, Heiden A, Scharfetter J, Moser E, Kasper S. Myo-inositol in depressive and healthy subjects determined by frontal ^{1}H-magnetic resonance spectroscopy at 1.5 tesla. J Psychol Res 1998;32:411-420
11. Berridge MJ, Irvine RF. Inositol phosphates and cell signaling. Nature 1989;41:197-205
12. Shimon H, Agam G, Belmaker RH, Hyde TM, Kleinman JE. Reduced frontal cortex inositol levels in postmortem brain of suicide victims and patients with bipolar disorder. Am J Psychol 1997;54:1148-1150
13. Moore GJ, Bebchuk JM, Parrish JK, Faulk MW, Arfken CL, Strahl-Bevacqua J, Manji HK. Temporal dissociation between lithium-induced changes in frontal lobe myo-inositol and clinical response in manic-depressive illness. Am J Psychol 1999;156:1902-1908
14. Lenox RH, Watson and DG. Lithium and the brain: a psychopharmacological strategy to a molecular basis for manic depressive illness. Clin Chem 1994;40:309-314
15. Michaelis T, Merboldt KD, Bruhn H, Frahm J. Absolute concentrations of metabolites in the adult human brain in vivo: quantification of localized proton MR spectra. Radiology 1993;187:219-227
16. Choi CG, Frahm J. Localized proton MRS of the human hippocampus: metabolite concentrations and relaxation times. Magn Reson Med 1999;41:204-207
17. Bruhn H, Stoppe G, Staedt J, Merboldt KD, Frahm J. Quantitative proton MRS in vivo shows cerebral myo-inositol and cholines to be unchanged in manic-depressive patients treated with lithium. Proc ISMRM New York 1993;p.1543
18. Behar KL, Rothman DL, Spencer DD, Petroff O.A.C. Analysis of macromolecule resonances in ^{1}H NMR spectra of human brain. Magn Reson Med 1994;32:294-302
19. Seeger U, Mader I, Nagele T, Grodd W, Lutz O, Klose U. Reliable detection of macromolecules in single-volume ^{1}H NMR spectra of the human brain. Magn Reson Med 2001;45:948-954
20. Hofmann L, Slotboom J, Boesch C, Kreis R. Characterization of the macromolecule baseline in localized ^{1}H-MR spectra of human brain. Magn Reson Med 2001;46:855-863
21. Kim H, Thompson RB, Hanstock CC, Allen PS. The Variability of Metabolite Yield Using STEAM or PRESS Sequences In Vivo at 3.0T Illustrated with Myo-Inositol. Magn Reson Med 2005;53:760-769
22. Sorensen OW, Eich GW, Levitt MW, Bodenhausen G, Ernst RR. Product operator formalism for the description of NMR pulse experiments. Prog NMR Spec 1983;16:163-192
23. Thomson RB, Allen PS. A new multiple quantum filter design procedure for use on strongly coupled spin systems found in vivo: its application to glutamate. Magn Reson Med 1998;39:762-771
24. Ross BD. Biochemical considerations in ^{1}H spectroscopy. Glutamate and glutamine; Myo-inositol and related metabolites. NMR Biomed 1991;4:59-63
25. Rothman DL, Petroff OAC, Behar KL, Mattson RH. Localized

^{1}H NMR measurements of γ-aminobutyric acid in human brain in vivo. Proc Natl Acad Sci USA 1993;90:5662-5666

26. de Graaf RA, Rothman DL. Detection of γ-aminobutyric acid (GABA) by longitudinal scalar order difference editing. J Magn Reson 2001;152:124-131
27. Keltner JR, Wald LL, Ledden PJ, Chen YI, Matthews RT, Baker JR, Rosen BR, Jenkins BG. A localized double-quantum filter for the in vivo detection of brain glucose. Magn Reson Med 1998;39:651-656
28. Keltner JR, Wald LL, Frederick BB, Renshaw PF. In vivo detection of GABA in human brain using a localized double-quantum filter technique. Magn Reson Med 1997;37:366-371
29. Lei H, Peeling J. A localized double-quantum filter for in vivo detection of taurine. Magn Reson Med 1999;42:454-460
30. McLean MA, Busza AL, Wald LL, Simister RJ, Barker GJ, Williams SR. In vivo GABA+ measurement at 1.5 T using a PRESS localized double quantum filter. Magn Reson Med 2002;48:233-241
31. Wilman AH, Allen PS. Double-quantum filtering of citrate for in vivo observation. J Magn Reson B 1994;105:58-60
32. Lei H, Peeling J. Simultaneous spectral editing for γ-aminobutyric acid and taurine using double quantum coherence transfer. J Magn Reson 2000;143:95-100
33. Trimble LA, Shen JF, Wilman AH, Allen P S. Lactate editing by means of selective-pulse filtering of both zero-and double-quantum coherence signals. J Magn Reson 1990;86:191-198
34. Wilman AH, Allen PS. Yield enhancement of a double-quantum filter sequence designed for the edited detection of GABA. J Magn Reson B 1995;109:169-174
35. Trabesinger AH, Weber OM, Duc CO, Boesiger P. Detection of glutathione in the human brain in vivo by means of double quantum coherence filtering. Magn Reson Med 1999;42:283-289
36. Sotak CH, Freeman DM, Hurd RE, The unequivocal detection of in vivo lactic acid using two-dimensional double quantum coherence-transfer spectroscopy. J Magn Reson 1988;78:355-361
37. Jouvensal L, Carlier PG, Bloch G. Practical implementation of single-voxel double-quantum editing on a whole-body NMR spectromenter: localized monitoring of lactate in the human leg during and after exercise. Magn Reson Med 1996;36:487-490
38. Wilman AH, Allen PS. The response of the strongly coupled AB system of citrate to typical ^{1}H MRS localization sequences. J Magn Reson B 1995;107:25-33
39. Lindon JC, Baker DJ, Farrant RD, Williams JM. ^{1}H, ^{13}C and ^{31}P n.m.r. spectra and molecular conformation of myo-inositol 1,4,5-triphosphate. Biochem J 1986;233:275-277
40. Behar KL, Ogino T. Assignment of resonances in the ^{1}H spectrum of rat brain by two-dimensional shift correlated and J-resolved NMR spectroscopy. Magn Reson Med 1991;17:285-303,
41. Matson GB. An integrated program for amplitude-modulated rf pulse generation and re-mapping with shaped gradients. Magn Reson Imaging 1994;12:1205-1225
42. Thomson RB, Allen PS. Sources of valiability in the response of coupled spins to the PRESS sequence and their potential impact on metabolite quantification. Magn Reson Med 1999;41:1162-1169
43. Thomson RB, Allen PS. Response of Metabolites with Coupled spins to the STEAM Sequence. Magn Reson Med 2001;45:955-965
44. Ernst RR, Bodenhausen G, Wokaun A. Principles of nuclear magnetic resonance in one and two dimensions, Oxford Science Publications, 1997
45. Kreis R, Ernst T, Ross BD. Absolute quantitation of water and metabolites in the human brain. II. Metabolite concentrations. J Magn Reson B 1993;102:9-19
46. Provencher SW. Estimation of metabolite concentrations from localized in vivo proton NMR spectra. Magn Reson Med 1993;30:672-679
47. Hore PJ. Solvent suppression in fourier transform nuclear magnetic resonance. J Magn Reson 1983;55:283-300
48. Morris GA, Freeman R. Selective excitation in fourier transform nuclear magnetic resonance. J Magn Reson 1978;29:433-462
49. Trabesinger AH, Mueller DC, Boesiger P. Single-quantum coherence filter for strongly-coupled spin systems for localized ^{1}H NMR spectroscopy. J Magn Reson 2000;145:237-245

대한자기공명의과학회지 13:117-126(2009)

인체 내 *myo*-Inositol 검출을 위한 수치해석적 이중양자 필터 디자인

가천의과학대학교, 이길여암당뇨연구원

이윤정 · 정진영 · 노형준 · 유웅식 · 김현진

목적: 수치해석적인 방법을 통해 핵자기공명 분광기법에서의 다중양자 필터를 디자인하는 방법을 소개하고 이를 뇌의 중요한 대사체인 *myo*-inositol 의 생체 내 검출에 이용하였다.
대상 및 방법: 이를 위해 우선적으로 *myo*-inositol 의 분광학적 성질을 조사 한 후 다중양자 필터의 echo time, mixing time 그리고 세번째 90° 펄스의 flip angle과 offset frequency같은 시퀀스 파라미터들을 최적화 하였다. 최적화된 필터는 우선적으로 실험 팬텀에서 테스트 한 후 최종적으로 인간의 두뇌에서 그 성능을 검증하였다.
결과: 실험결과를 토대로, 본 연구에서 제안하는 다중양자 필터를 사용하여 신호의 순수도가 크게 개선된 타겟 대사체의 신호를 얻을 수 있음을 알 수 있다.
결론: 수치해석적인 방법을 통하여 핵자기공명 분광기법에서의 다중양자 필터를 디자인함으로써 특히, 복잡한 스핀계를 갖는 타겟대사체의 신호의 순수도를 크게 강화할 수 있다.

통신저자 : 김현진, 유웅식, (406-840) 인천시 연수구 송도동 7-45, 가천의과학대학교 이길여암당뇨연구원
Tel. 032-899-6060, 6058 Fax. 032-899-6058 E-mail: hkim@gachon.ac.kr, ungsik@gachon.ac.kr